

A numerical scheme for modeling tidal wetting and drying

S. Lahaye,¹ F. Gouillon,² R. Baraille,² A. Pichon,³ L. Pineau-Guillou,³ and Y. Morel²

Received 17 September 2010; revised 16 December 2010; accepted 14 January 2011; published 30 March 2011.

[1] This paper introduces a numerical scheme developed to model the wetting and drying of coastal areas by the tide, suitable for an oceanic circulation model using finite differences. It is based on existing numerical schemes developed for isopycnic models for which the layer thickness can vanish when they interact with the bottom topography. Some original features are added and the scheme is optimized to accurately reproduce analytical solutions of an idealized problem. The main parameters of this numerical scheme are (1) a critical height, which depends on the local bottom slope and the grid step, and (2) the Rossby number. This original numerical scheme is applied to a realistic barotropic configuration of the Normand-Breton Gulf where tidal amplitudes are large and where the wet/dry front location varies greatly.

Citation: Lahaye, S., F. Gouillon, R. Baraille, A. Pichon, L. Pineau-Guillou, and Y. Morel (2011), A numerical scheme for modeling tidal wetting and drying, *J. Geophys. Res.*, 116, C03028, doi:10.1029/2010JC006666.

1. Introduction

[2] The numerical modeling of coastal regions has recently gained considerable attention in the oceanography community. It is now necessary to take into account the particular dynamics of coastal region within high-resolution (i.e., few kilometers) basin-scale circulation models. To do so, primitive equation models developed in the context of modeling the deep ocean are used sometimes without any significant change to their numerical schemes. This is convenient and adequate for many oceanic coastal regions. However, even when using fine model grid spacing, some processes are not represented and need to be parameterized or adapted. This is the case of the wetting and drying process. In regions where the tide is important, the treatment and the representation of the wetting and drying process within the model is crucial to have an accurate description of the local dynamics.

[3] The wetting and drying problem in shallow water equations has been intensively studied during the last 20 years in particular for coastal engineering applications [Balzano, 1998; Lynett *et al.*, 2002; van't Hof and Vollebregt, 2005, and references therein] using finite element or finite volume approaches. This problem can be handled either by (1) dynamically adapting the mesh according to the position of the wet/dry interface (the calculation grid moves [Lynch and Gray, 1980]) or (2) by resolving the equations on a fixed grid with the issue of partially wet cells addressed by using appropriate numerical methods [Leclerc *et al.*, 1990; Bradford and Sanders, 2002; Begnudelli and Sanders, 2006]. The case (1) has been intensively studied until the end of the 90s. The methods related to (1) generally consist in three steps: the first step is the determination of the position of the

wet/dry interface, the second step is a remeshing step, and the last step consists of a projection of the variables onto the new mesh. The computational cost of (1)-like methods is very high thus the use of algorithms related to case (2) is preferable for general applications. The modeling community has also focused on solving wetting and drying problems on fixed numerical grids. A general review of the numerical algorithms used for (2)-like methods are given by Bates and Horritt [2005] and Balzano [1998] where several methods averaging the water depth at the cell interface on an Arakawa C grid are compared. In order to avoid spurious oscillations on the velocity, Hervouet and Janin [1994] and Benkhaldoun and Monthe [1994] cancel the topography gradient term in partly flooded cells. Aureli *et al.* [2008] propose the combination of two Monotonic Upstream centered Scheme for Conservation Laws (MUSCL), one for the surface elevation and one for the water depth, with respect to the local Froude number. These previous studies mainly concentrated on the representation of an accurate surface elevation. Although they validated their results for the simulated surface elevation, they did not for the velocity fields.

[4] Modeling the wetting and drying has however rarely been undertaken in coastal circulation models using finite difference methods. Examples are given by Lazure and Salomon [1991], Lazure and Jegou [1998], and Oey [2005, 2006] which are, to our knowledge, the only studies with the development of a numerical scheme taking into account the wetting and drying processes in oceanic circulation models using a finite difference framework. Numerical methods using finite element and finite volume have inspired finite difference model developers, which now use numerical schemes globally conserving mass, energy, enstrophy, and tracers quantity (a property which is inherent to finite volume models). This is the case of the Miami Isopycnic Coordinate Ocean Model (MICOM [Bleck and Smith, 1990; Bleck *et al.*, 1992]) and of the Hybrid Coordinate Ocean Model (HYCOM [Bleck, 2002]). In particular, stimulated by the finite element/volume approach, specific numerical

¹CEA/DEN, Gif-sur-Yvette, France.

²SHOM, HOM, Toulouse, France.

³SHOM, HOM, Brest, France.

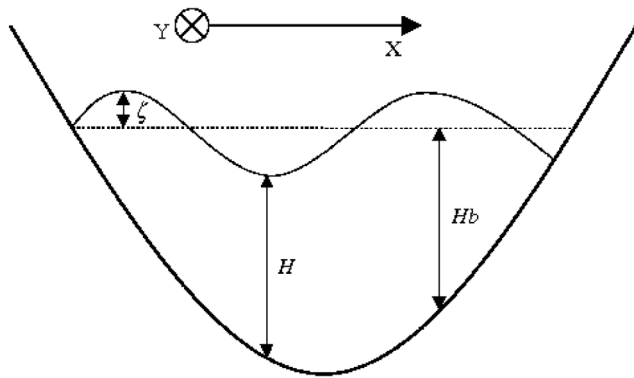


Figure 1. Schematic of the idealized configuration used. Based on *Thacker* [1981].

schemes dealing with the intersection between layers and topography (i.e., vanishment of internal layers) have already been implemented in the MICOM and HYCOM codes to calculate the baroclinic pressure gradient.

[5] The main goal of the present study is to propose an original numerical scheme to represent wetting and drying processes. This scheme can be used for the resolution of the barotropic conservation laws in general oceanic circulation models using finite differences. In contrast to the aforementioned studies, we focus on the analysis of both the surface elevation and velocity field obtained using the new numerical scheme, insisting on the velocity field for transport and drift applications. By representing accurately the wetting and drying process in finite difference oceanic circulation models, it could lead to more accurate numerical solutions in coastal regions.

[6] To develop and test numerical schemes, it is interesting to compare the numerical solutions of idealized problems to their analytical reciprocity. There are not many known analytical solutions for wetting and drying configurations but *Thacker* [1981] has found some exact solutions for the non-linear shallow water equations in 1-D and 2-D in parabolic basins. These analytical solutions can be fruitfully used to evaluate the accuracy of the representation of the wetting and drying process [*Balzano*, 1998; *Lynett et al.*, 2002].

[7] In section 2, we present and describe the numerical algorithm we have developed, and in section 3 we discuss its optimization and limitation by comparing the numerical scheme results to the *Thacker's* analytical solutions. In section 4, an application to a regional coastal model of the Manche is also presented.

2. Numerical Algorithm

2.1. Equations

[8] We consider the 2-D shallow water equations [*Cushman-Roisin*, 1994] which can be written

$$\begin{aligned} \partial_T U + (\mathbf{U} \cdot \nabla) U - f_o V &= -g \partial_X (H - Hb) + F_X, \\ \partial_T V + (\mathbf{U} \cdot \nabla) V + f_o U &= -g \partial_Y (H - Hb) + F_Y, \\ \partial_T H + \text{div}(HU) &= 0, \end{aligned} \quad (1)$$

where $\mathbf{U} = (U, V)$ represents the horizontal components of the velocity field, f_o is the local Coriolis parameter, g is the earth gravity, H is the water column thickness, Hb is the position of the bottom, $H - Hb$ is the sea surface height (SSH) and also define as ζ in Figure 1, and F_X and F_Y are dissipation terms. The dissipation terms are split into $\mathbf{F} = \text{Diff}(\mathbf{U}) + \Theta$, where $\mathbf{F} = (F_X, F_Y)$, $\text{Diff}(\mathbf{U})$ is of numerical origin and needed to avoid the development of small-scale noise, and Θ is associated with the parameterization of physical dissipation processes (e.g., bottom friction). The wetting and drying process is associated with shocks in the velocity field as the point where the thickness vanishes is usually associated with a velocity discontinuity. The advection terms solved using centered schemes are dispersive (i.e., creation of numerical oscillations) and shocks generally generate large-grid-scale noise that can contaminate the results. To deal with shocks, harmonic or biharmonic viscosity has to be used with a viscosity parameter depending on the deformation tensor [*Smagorinsky*, 1963; *Winther et al.*, 2007]. For the academic configuration used in this study and presented in section 3, an harmonic operator has been used (our model configuration did not allow the use of a biharmonic diffusion operator) and is defined as

$$\text{Diff}(\mathbf{U}) = \partial_X(\nu \partial_X \mathbf{U}) + \partial_Y(\nu \partial_Y \mathbf{U}), \quad (2)$$

with

$$\nu = C_s \Delta X^2 \text{defor}, \quad (3)$$

with $\text{defor} = \sqrt{(\partial_X U - \partial_Y V)^2 + (\partial_Y U + \partial_X V)^2}$, the deformation tensor, ΔX is the grid step, and C_s is the Smagorinsky coefficient with $C_s = 0.05$ (see *Winther et al.* [2007] for justification). However, for the more realistic configuration of the Normand-Breton Gulf, we use a biharmonic operator define as

$$\text{Diff}(\mathbf{U}) = \partial_X(\nu' \partial_X^3 \mathbf{U}) + \partial_Y(\nu' \partial_Y^3 \mathbf{U}), \quad (4)$$

with

$$\nu' = C_s \Delta X^4 \text{defor}. \quad (5)$$

[9] In addition, for the more realistic configuration, the bottom friction has to be taken into account in the dissipation term. In a 3-D model, the frictional forcing is represented as the vertical derivative of a stress assumed to be equal to the stress at the boundary and linearly decreasing to zero over a critical thickness chosen to be approximately 10 m [*Bleck and Boudra*, 1986]. The bottom stress (τ) follows a quadratic law and is given by

$$\tau = -\rho C_d |U| U, \quad (6)$$

where ρ is the density, and C_d is a drag coefficient ($C_d = 0.003$). For the barotropic case considered here, the effect of bottom friction is then given by

$$\Theta = -\frac{C_d |U| U}{H}. \quad (7)$$

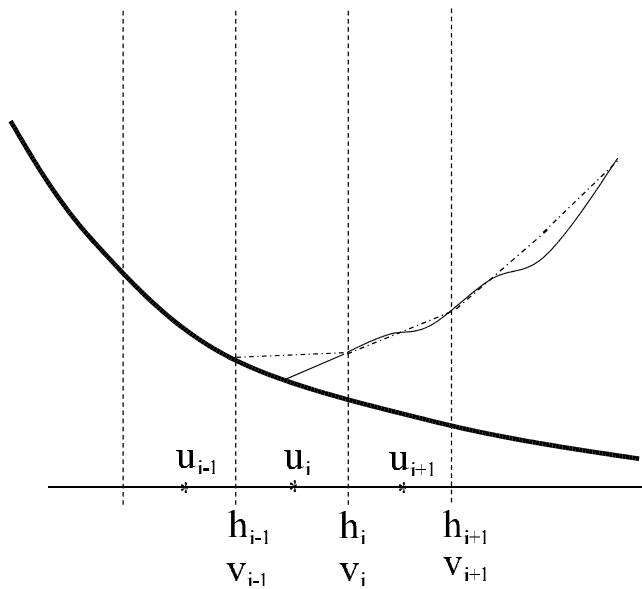


Figure 2. Schematic of the discretized grid. The thick black line is the bottom topography, the thin black line is the real free surface, and the dashed line is the numerical free surface. Notice the inaccuracy where the free surface intersects the bottom, which can lead to errors in the calculation of the SSH (i.e., pressure) gradient term.

[10] In the first part of this study, we consider a 1-D model and assume that $\partial_Y = 0$. The resulting 1-D shallow water equations are then

$$\begin{aligned} \partial_T U + U \partial_X U - f_o V &= -g \partial_X (H - Hb) + F_X, \\ \partial_T V + U \partial_X V + f_o U &= F_Y, \\ \partial_T H + \partial_X (HU) &= 0. \end{aligned} \quad (8)$$

2.2. Numerical Schemes

[11] In most oceanic general circulation models, equation (1) or equation (8) are generally solved on a C grid [Arakawa and Lamb, 1977]. Isopycnic models have a long history for dealing with vanishing layers as isopycnic layers often outcrop bottom topography and need to disappear [Bleck and Boudra, 1986; Bleck and Smith, 1990; Bleck et al., 1992], a problem for which, numerical algorithms have been developed and tested and which is similar to the wetting and drying of a land. Figure 2 shows the associated numerical problems and a zoom of an idealized region where the water column depth vanishes. It underlines the problem of non-physical velocity points as they are associated with the absence of the fluid. As a result the velocity of these grid points should not be used in the numerical calculations. It also shows that the SSH (or pressure) gradient at the first velocity point inside the physical region has to be carefully evaluated to avoid taking into account the bottom topography gradient instead of the sea surface elevation one.

[12] In addition, the fluid thickness has to remain non-negative, a property that is not verified by common schemes

(e.g., centered schemes) but there exists other numerical schemes ensuring positivity (e.g., flux corrector schemes).

[13] As mentioned in section 1, all the previous problems have already been identified and dealt with in isopycnic models and we thus base our approach on these available, robust, and computationally efficient numerical schemes.

2.2.1. Continuity Equation

[14] To keep the layer thicknesses positive when the layers become very thin or even vanish, it is necessary to use the upwind scheme, which is a positive definite scheme. The upwind scheme is however known to be very diffusive, and it should thus be restricted to areas where it is needed. Its combination with a higher order, but not positive definite scheme, is thus a good compromise for the calculation of the thickness over the whole area. There exists a few numerical schemes combining the upwind scheme to higher-order (generally second-order) schemes so as to preserve positive thicknesses [Zalesak, 1979; Smolarkiewicz, 1983]. In this study, we have chosen the Zalesak scheme for the computation of the barotropic continuity equation.

2.2.2. SSH Gradient

[15] The only way to deal with the SSH gradient calculation, intervening in equation (1) or equation (8), is to extrapolate the gradient from neighboring physical (i.e., wet) region to the region where there exists a point with zero water thickness. The resulting SSH gradient for the velocity points neighboring a zero thickness point is then calculated at first order but remains close to its physical value. This method has been successfully used in the MICOM and HYCOM models [Bleck and Smith, 1990]. The idea is to average the SSH gradients of all direct neighboring points with a weight proportional to the layer thickness when below a critical thickness hc^P

$$\begin{aligned} w_i &= \min(hc^P, H_i, H_{i-1}), \\ \text{grad}(\zeta)_i^U &= \frac{w_i(\zeta_i - \zeta_{i-1})/\Delta X + (hc^P - w_i)\overline{\nabla}\zeta_i}{hc^P}, \end{aligned} \quad (9)$$

where the superscript U in $\text{grad}(\zeta)_i^U$ means the gradient is calculated on a velocity point (Figure 2) and

$$\overline{\nabla}\zeta_i = \frac{w_{i-1}(\zeta_{i-1} - \zeta_{i-2})/\Delta X + w_{i+1}(\zeta_{i+1} - \zeta_i)/\Delta X}{\epsilon^P + w_{i-1} + w_{i+1}}, \quad (10)$$

where the index notation is defined in Figure 2.

[16] Notice the two parameters in the latter scheme hc^P and ϵ^P . hc^P represents the cutoff thickness below which an average of the SSH gradient term is taken into account. ϵ^P is the damping thickness (below, the average gradient is damped toward zero). These two parameters have to be adjusted for the general case.

2.2.3. Coriolis and Advection Terms

[17] A special treatment is also necessary to avoid using the Coriolis and advection terms when they are computed using velocity values coming from the nonphysical domain (i.e., dry region). Contrarily to the methods used in MICOM and HYCOM [Bleck and Boudra, 1986; Bleck and Smith, 1990], we adopt an elementary and cheap method: the Coriolis and advection terms are first calculated using the usual centered schemes and then included into the averaging procedure for the SSH gradient discussed above. The global

averaging procedure including all evolution terms except the dissipation leads to

$$\begin{aligned} w_i &= \min(hc^P, H_i, H_{i-1}), \\ evol_i^f &= \frac{w_i evol_i + (hc^P - w_i) \overline{evol}_i}{hc^P}, \\ \overline{evol}_i &= \frac{w_{i-1} evol_{i-1} + w_{i+1} evol_{i+1}}{\epsilon^P + w_{i-1} + w_{i+1}}, \\ evol_i &= -Advec_i - Corio_i - grad(P)_i, \end{aligned} \quad (11)$$

where $Advec_i$, $Corio_i$, and $grad(P)_i$ are the advection, Coriolis, and surface pressure gradient terms, respectively, calculated for each (U, V) component on a specific point with a centered scheme. The dissipation term could also be averaged, but this has no effect on the simulations presented here. It can be explained by the additional nudging of the velocity field discussed in section 2.2.4.

2.2.4. Final Nudging of the Velocity Field

[18] The previous procedure allows for the limitation of errors when calculating the velocity evolution terms in the physical region. When a point is dry, it might acquire unrealistic velocity magnitudes that rapidly diverge from the realistic values of the physical region. This can cause problems if the point eventually becomes wet. To solve this issue, it is necessary to constrain the velocity field in dry areas to ensure velocity magnitudes approaching the ones of the nearby wet points. This is achieved by developing a nudging scheme for the velocity field toward neighboring point values. Tests with other methods (e.g., no constraints, nudging toward zero) have shown that this was by far the best choice. The nudging procedure is

$$\begin{aligned} w_i &= \min(hc^U, H_i, H_{i-1}), \\ U_i^f &= \frac{w_i U_i + (hc^U - w_i) \overline{U}_i}{hc^U}, \end{aligned} \quad (12)$$

where U_i is the velocity at index i calculated from the momentum equations (using the schemes presented in section 2.2.3), U_i^f is its final and averaged value, and \overline{U}_i is given by

$$\overline{U}_i = \frac{w_{i-1} U_{i-1} + w_{i+1} U_{i+1}}{\epsilon^U + w_{i-1} + w_{i+1}}. \quad (13)$$

[19] Notice the two new parameters hc^U and ϵ^U which have to be adjusted for the general case. In order to do so, we use analytical solutions derived by *Thacker* [1981].

3. Optimizing the Model Parameters Using an Idealized Problem

[20] We have defined four parameters that we reduce to three (tests conducted with hc^U not equal to hc^P did not improved the solutions): $hc = hc^U = hc^P$, ϵ^U , and ϵ^P . These parameters have to be carefully chosen to avoid numerical problems (e.g., numerical noise) and to give accurate solutions. If hc is chosen too small, the nonphysical solutions are increasing and spreading within the physical domain, and might lead to a model blow up. If hc is chosen too large, the solution is unnecessarily damped and loses accuracy.

A value of hc for which the model is stable for all configurations and domains, probably leads to the case of damped and inaccurate solutions. The three aforementioned parameters could be chosen using specific tests for each configurations. In this study, using analytical solutions, we determine the parameters optimized value as a function of few parameters.

3.1. Thacker's Solutions

[21] *Thacker* [1981] has found exact inviscid analytical solutions for both equation (1) and equation (8) for which some areas are periodically dried and wetted again. Oscillating solutions have been found for parabolic basins whose depths are given by

$$Hb = D_o \left(1 - \left(\frac{x}{L} \right)^2 \right), \quad (14)$$

where D_o is the maximum depth of the domain, and L is half the length of the basin (where the water thickness is not null). The pulsation period is constant and given by:

$$\omega = \sqrt{f_o^2 + \frac{2gD_o}{L^2}}. \quad (15)$$

[22] To deal with the general case, it is convenient to use nondimensional equations and use the following nondimensional variables

$$\begin{aligned} x &= \frac{X}{L}, \\ h &= \frac{H}{D_o}, \\ d &= \frac{D}{D_o}, \\ t &= \omega T, \\ u &= \frac{U}{\omega L}, \\ v &= \frac{V}{\omega L}. \end{aligned} \quad (16)$$

[23] Equation (8) then becomes

$$\begin{aligned} \partial_t u + u \partial_x u - R_o v &= -Bu \partial_x (h - hb) + F_x, \\ \partial_t v + u \partial_x v + R_o u &= F_y, \\ \partial_t h + \partial_x (hu) &= 0, \end{aligned} \quad (17)$$

where

$$\begin{aligned} Bu &= \frac{gD_o}{\omega^2 L^2}, \\ R_o &= \frac{f_o}{\omega}, \\ &= \sqrt{1 - 2Bu}. \end{aligned} \quad (18)$$

[24] Equation (17) is thus monitored by a single parameter Bu representing the influence of the coriolis effect versus the

gravity effects. Notice that for the nonrotating case ($f_o = 0$), $R_o = 0$ and $Bu = 1/2$. The Thacker's solutions we have used in this study are

$$\begin{aligned} hb &= 1 - x^2, \\ u &= -\eta \sin(t), \\ v &= -\eta f \cos(t), \\ h &= 1 - x^2 + 2\eta \cos(t) \left(x - \frac{\eta}{2} \cos(t) \right), \end{aligned} \quad (19)$$

where η is a parameter characterizing the nondimensional amplitude of the periodic motion. The shoreline is given by $x = \eta \cos(t) \pm 1$, so that 2η represents the total distance over which land periodically dries and wets on each side of the basin.

[25] Thacker's study provides a useful set of analytical solutions to validate a numerical solution of the wetting and drying process. It also allows for the optimization of the numerical schemes dedicated to the wet and dry process. Thacker's solutions depend mainly on the parameter η , but also on the nondimensional local slope $\partial hb/\partial x = s$ (where land periodically wets and dries $s \sim 2$). Another important parameter is Bu , which is the only parameter of the nondimensional equation (17) (dissipation excluded), and finally, the parameters characterizing the numerical discretization, Δx and Δt , representing the nondimensional grid step and time step, respectively, have to be considered too. Thus the coefficients $hc^U = hc^P$, ϵ^U and ϵ^P depend a priori on five parameters. Studying the dependency of each coefficient to each parameter is cumbersome and thus, the parameter list needs to be reduced.

[26] First, we neglect the parameter Δt as it is associated with time derivative because we have seen that the main numerical problems arise from spatial schemes and not the temporal ones. Figure 2 also shows that an elementary cell can be dried when its thickness is less than $s\Delta x$ (where s is the local bottom slope). Thus the important parameter is $\Delta h = s\Delta x$ and we define $hc^U = hc^P = \alpha\Delta h$, $\epsilon^U = \alpha^U hc^U$ and $\epsilon^P = \alpha^P hc^P$, and calculate the best α coefficients and their dependency on the parameters Bu and η .

[27] To investigate the sensitivity of the numerical scheme and find optimized value for this specific configuration, we compare the numerical and analytical solutions considering the following fields: (1) mean currents (time averaged over the seiche period), (2) mean transports (time averaged over the seiche period), (3) accuracy of the velocity field in the wetting and drying region, and (4) the conservation of the amplitude (measured in the middle of the domain).

[28] The mean currents and mean transports for Thacker's solutions are nonzero as they have to be calculated over the physical region. In the regions of wetting and drying, the time mean of the considered field has to be calculated over the time period when $h > 0$ and not during the whole period of the oscillations. When f is different from zero, this method yields to a zero mean for u and hu but not for v and hv .

3.2. The Nonrotating Case

[29] When $f = 0$, $v = 0$ and $Bu = 1/2$ is constant, and η is the only remaining parameter in equation (17). Figure 3

shows the results for the reference experiment where the values for the considered parameters are given by

$$\begin{aligned} \Delta x &= 0.005, \\ \Delta t &= 0.0025, \\ \eta &= 8\Delta x, \\ \alpha &= 2, \\ \alpha^U &= 0.01, \\ \alpha^P &= 0.01. \end{aligned} \quad (20)$$

[30] Figure 3 shows the results of the reference experiment run for 10 oscillation periods with parameters defined in equation (20). The analytical (dashed lines) and numerical (solid lines) solutions are plotted for the velocity field in the vicinity of the wetting/drying region during the last oscillation (Figure 3a), the time average of the velocity field (Figure 3b), and the time evolution of the error (root mean-spatial mean square) of the layer depth (Figure 3c) and the transport hu (Figure 3d). There is a slight overshoot in the simulated velocity field compared to the predicted velocity field, but the two solutions are similar (Figure 3a). A mean current develops in the wetting drying region because of the damping we impose (Figure 3b). However, this region is associated with small layer depth, thus the associated local transport is very low. The mean current reaches $u = 20 \times 10^{-5}$ after the 10 oscillation periods which is small compared to the maximum velocity in this region $U_{\max} = \eta = 0.04$. For the realistic configurations the mean currents can be of importance if one is interested in the long-term drift of tracers or particles. It is necessary to evaluate the "numerical drift" and compare its magnitude to the observed velocity drift magnitude (due to tidal rectification, winds, etc.) If this numerical drift is not negligible, the only method to alleviate it is to reduce the model grid step in the wetting and drying region.

[31] Figure 4 shows the position of the simulated shoreline with respect to time and compares it to the analytical position of the shoreline. Results show that the predicted and simulated solution of the shoreline location compare well. The model has a slight shift toward the shallow waters (approximately representing two grid points) which happens early in the run. This is probably due to the approximations and necessary damping associated with the numerical scheme in the area where h becomes small. At the position of the analytical shoreline (2 grid points below), the water depth is $h = 0.002 = 0.2s\Delta x$. This is small if the wetting and drying region extends over several grid points: the height variation in this region is then much bigger than $s\Delta x$. For example, if the wetting and drying region extends over one grid point, then the error represents only about 10%.

[32] Numerical experiments have also been performed with different triplets (α , α^U , α^P) to investigate the optimal value range for these parameters. Results show that there does not exist a precise optimal values for these parameters but a range of values. The most sensitive value is α , for which the best results are obtained with $\alpha \in [1, 2]$. Figure 5 shows the impact of varying the parameter from the refer-

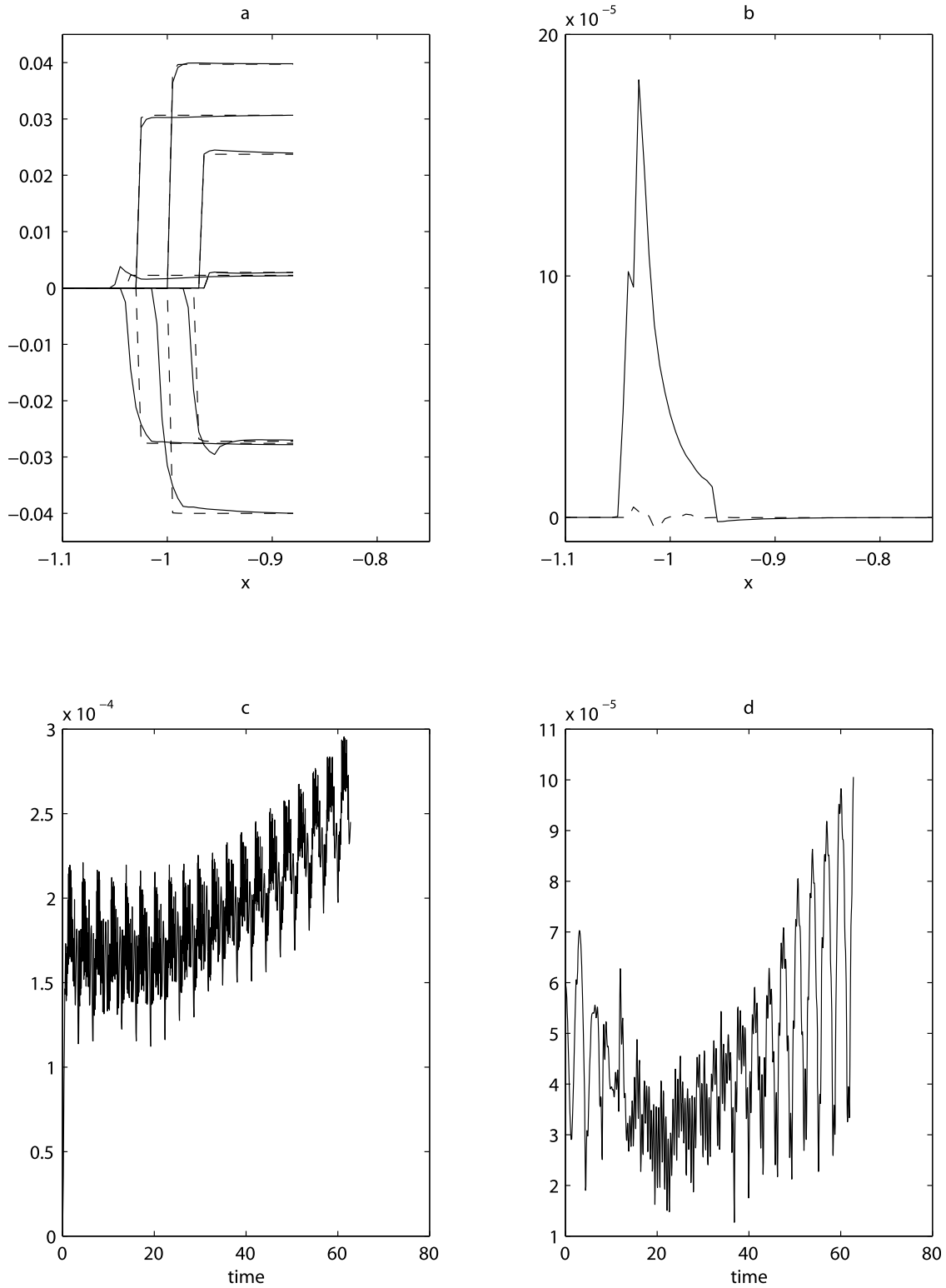


Figure 3. Comparison between the analytical solution (dashed line) and the numerical (solid line) solution for (a) the velocity fields at different times, (b) the mean velocity, (c) the time evolution of the error (root mean square) of the layer depth, and (d) the time evolution of the error (root mean square) of the transport.

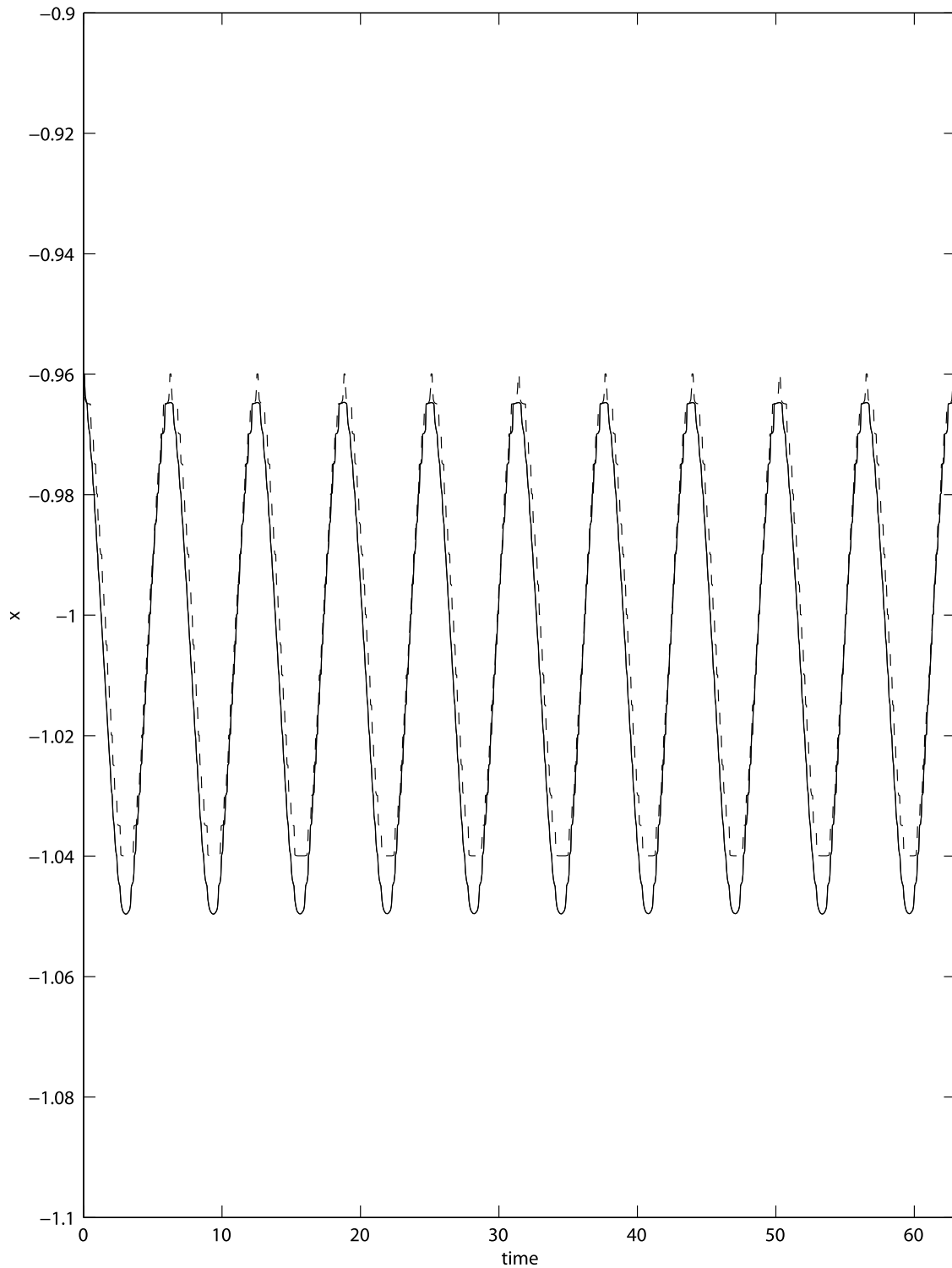


Figure 4. Position of the shoreline for the analytical solution (dashed line) and the simulated position of the shoreline (solid line, defined by $h \leq 10^{-2}\eta$).

ence experiment (where $\alpha = 2$, solid lines) on different diagnostics. Results show that the simulated velocity field, transport and layer thickness compare better to their analytical reciprocity when $\alpha = 2$ which is the reference case. The experiments using larger α value ($\alpha = 4$, dashed lines) and lower α value ($\alpha = 0.5$, dotted lines) show larger errors. The case of $\alpha = 1$ is better for the conservation of the

free surface amplitude (result not shown here) but $\alpha = 2$ represents better the velocity field in the wetting and drying regions. When $\alpha = 2$, the solution is more robust as it leads to a SSH damping over a wider region. In realistic configurations, wetting and drying regions are generally associated with an external forcing (generally the tide) which maintains the amplitude of the oscillation in the long-term. Local

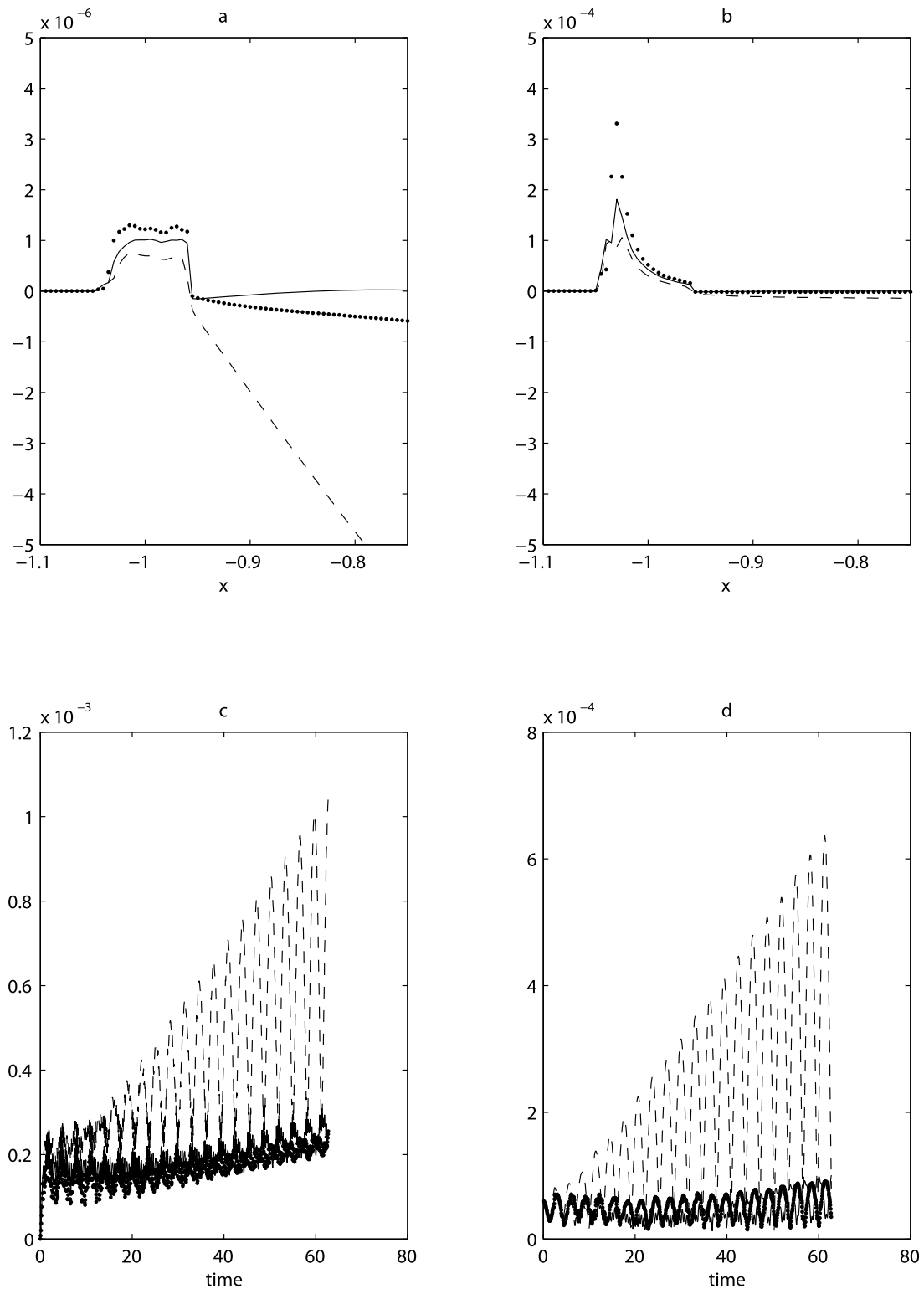


Figure 5. Impact of varying the parameter α from $\alpha = 2$ (reference experiment, solid line) to $\alpha = 0.5$ (dotted line) and $\alpha = 4$ (dashed line) on (a) the time average of the difference between analytic and numerical transport, (b) the time average of the difference between analytic and numerical velocity, (c) the time evolution of the root mean square error of the layer thickness, and (d) the time evolution of the root mean square error of the transport.

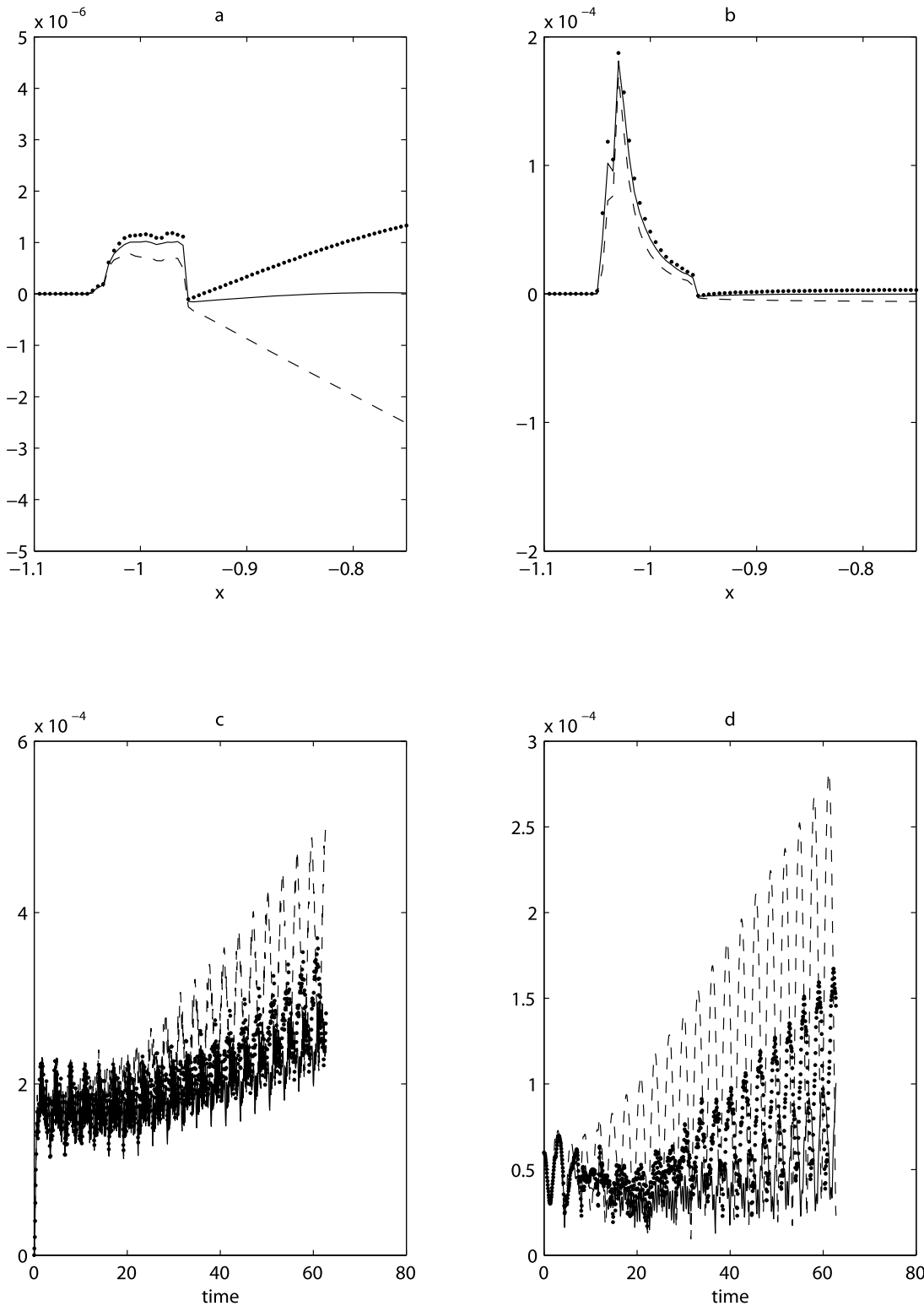


Figure 6. Same as Figure 5 but varying the α^U . The solid line is $\alpha^U = 0.01$ (reference experiment), the dotted line is $\alpha^U = 0.005$, and the dashed line is $\alpha^U = 0.02$.

accuracy, and robustness of the scheme, is thus a better property to achieve and the choice of $\alpha = 2$ is recommended for models used operationally. This particular choice of α would, however, not necessarily be optimal to model water running down a slope. Values taken away from this range

(i.e., $[1, 2]$) leads to inaccurate results. An optimum choice of α does not exist to provide better results for all choice of criterion.

[33] Figure 6 is the same as Figure 5 except that a sensitivity test of the model solution on the choice of α^U is

conducted. The reference experiment ($\alpha^U = 0.01$, solid lines) is compared to cases where $\alpha^U = 0.02$ (dashed lines) and $\alpha^U = 0.005$ (dotted lines). Results show again that the reference experiment leads to a better agreement with the analytical solution. Varying α^P does not impact the solution significantly (not shown here). For any α^P chosen less than 0.1 (but not zero), the results are similar and we thus define $\alpha^P = \alpha^U = 0.01$.

[34] As already mentioned in the introduction, in this study, we mainly focus and optimize the parameters for the velocity field for transport and drift applications. This could lead to degraded SSH (or layer thickness) evolution. In fact, the evolution of the SSH (or layer thickness) is indeed given by the divergence of the net transport, a quantity that is trivial to calculate, even with zero layer thickness, and, provided one uses positive schemes (such as Zalesak), no other transformation have to be performed on the SSH whose accuracy thus mostly depends on the accuracy of the velocity field. As explained above, things are more problematic for the velocity field for which it is necessary to deal with shocks for the velocity equation. The velocity field is thus the limiting factor and improving its accuracy improves the accuracy of the SSH. As shown in Figures 5 and 6 the optimum values for the velocity field are also optimum for the layer thickness (see panel c).

[35] We have checked that the accuracy of the SSH agrees with the analytical solution and the discrepancies are only located in the close vicinity of the shoreline (where the layer thickness becomes zero). As seen in Figure 4 there is a slight asymmetry for the accuracy of the shoreline (and SSH) evolution: the precision is better when the water flows offshore than when it flows onshore. This is due to the use of the upwind scheme (in the Zalesak algorithm) in areas with small water thickness and the fact that our scheme extrapolates the velocity field horizontally for the velocity point just after the shoreline. For water flowing offshore, the flux at the shoreline will be null (in agreement with the analytical expectation) whereas for onshore motion it will not which induces a rapid “wetting” of the next cell and an onshore displacement of the shoreline.

[36] Finally, sensitivity tests were conducted on the choice of values for parameters defined in equation (20) with respect to η and ΔX . The results show that larger amplitudes or model grid steps lead to stronger numerical errors. The accuracy of the results thus depends on η and ΔX but the optimum values for the α parameters to get the lowest errors remain unchanged and are thus independent of the model grid resolution and of the nondimensional oscillation amplitude.

3.3. Results for the Rotating Case

[37] When f is not equal to zero there exists an additional parameter Bu on which the previous parameters could depend. The previous experiments are conducted again with different values of Bu (i.e., varying the nondimensional Coriolis parameter R_o from 0 to 1, its maximum value). Notice that v is different from zero in this case so that the mean transport parallel to the coast is now an important process to test the accuracy of the scheme. Thacker’s solutions show that both the mean transport and mean velocity parallel to the coast are nonzero.

[38] There are no differences between the rotating case with small values of R_o and the nonrotating cases. For the

numerical experiments with moderate and large (close to one) value of R_o , results show that there exist one optimal choice for the α coefficients. We thus focus on the results given by a strong rotating case (i.e., $R_o = 0.9$) and we use identical parameters to the previous nonrotating reference experiment described above. Figures 7 and 8 show a comparison between the numerical solutions (plain lines) and analytical solutions (dashed lines) for the velocity u during the last oscillation period (Figure 7a), the mean (time average) current u (Figure 7b), the mean parallel current v (Figure 7c), and the mean parallel transport hv (Figure 7d), where $(\alpha, \alpha^U, \alpha^P) = (2, 0.01, 0.01)$, similar to the nonrotating experiment. The error on the mean simulated current u has been reduced and remains small compare to the nonrotating case. Although, the mean simulated current v is shifted inshore (two grid points) and smaller than the analytical mean current, it qualitatively compares well with the predicted solution. Its maximum value reaches 12×10^{-3} to be compared to the maximum instantaneous velocity of 36×10^{-3} . The mean simulated transport well agrees with the analytical solution of the mean transport, with a 10% error near the wetting drying region where the transport is the largest.

[39] Varying α yields to the same results as for the nonrotating case. Figure 9 shows the difference between the numerical and analytical solutions for three different choices of α . Diagnosing the meridional velocity, the temporal mean meridional transport, the spatial mean water thickness and transport show that the results are similar to the nonrotating case and that the optimal value choice for the parameter is still $\alpha = 2$ so that $hc^U = hc^P = 2s\Delta x$.

[40] Varying α does not significantly impact the solution as long as the value is smaller than approximately 0.1. However, there are significant differences when varying α^U . Results show that solutions are similar to the theory when $\alpha^U = 0.001$ (Figure 10). When $\alpha^U < 0.0005$, the simulation can become unstable and cause the model to blow up. For these cases, the mean parallel velocity and transport are improved (the two grid point shift still exists, but the maximum speed is closer to the analytical maximum speed).

[41] The Coriolis effect has thus a strong effect on the accuracy of the numerical scheme we discussed in section 3.2. When considering rotation, the parameter α^U is the only one that depends on Bu (i.e., R_o) and should be carefully chosen to maximize the accuracy of the numerical scheme. In practice for oceanic general circulation models, for which Coriolis is always considered and largely contributes to the regional ocean dynamics, the choice of $\alpha^U = 0.001$ is recommended.

[42] Thacker [1981] has also provided a set of solutions for 2-D cases, but they do not drastically differ from the 1-D solution (parabolic basin with a rotating flat free surface or a pulsating parabolic free surface). The optimized choices for the values of the different parameters of the 1-D case are also valid for the 2-D case.

4. A Realistic Case

[43] The previous numerical scheme can be easily adapted to a realistic configuration with tides. As the time period associated with the tides (diurnal and semidiurnal) is close to the inertial time period for most of the ocean then $R_o = f/\omega \simeq [0.5 - 1]$. Thus we choose $\alpha^U = 0.001$ to optimize the accuracy of the scheme. The parameter can be adapted to the

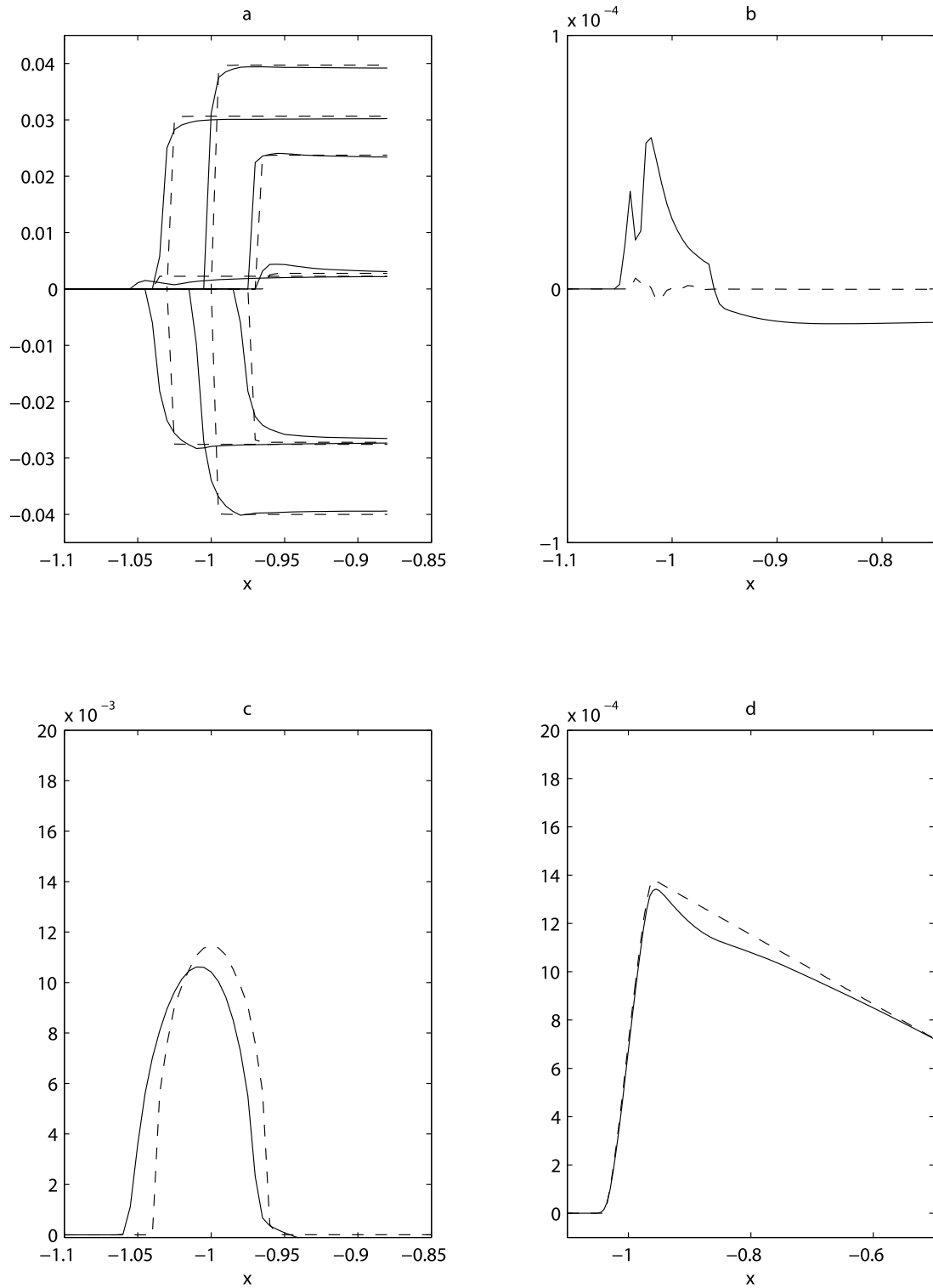


Figure 7. Analytical solutions (dashed line) and numerical solutions (solid line) for (a) the cross-shore velocity u at different times, (b) the mean cross-shore velocity, (c) the mean alongshore velocity, and (d) the mean alongshore transport.

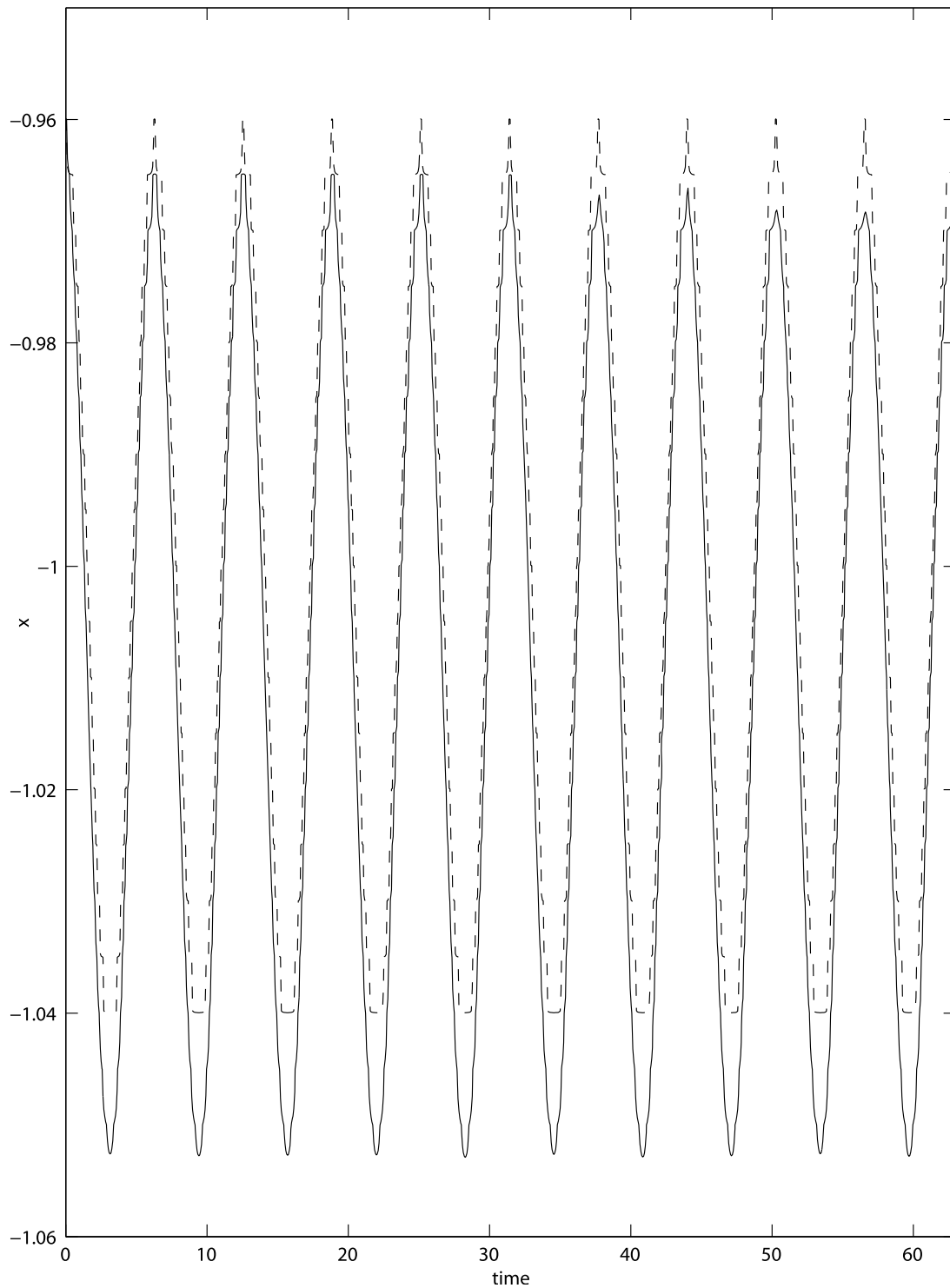


Figure 8. Position of the shoreline for the analytical solution (dashed line) and numerical one (solid line, defined by $h \leq 10^{-2}\eta$).

local bottom slope by defining $\alpha = 2$. In practice, to avoid problems over flat areas, we choose

$$hc^{\hat{U}} = hc^P = \sqrt{(h_{\min}^2 + (2s\Delta x)^2)}, \quad (21)$$

where $h_{\min} = 0.1$ m.

4.1. The Normand-Breton Gulf Configuration

[44] Along the northern French coast in the Manche (English Channel), the mean tide amplitude is approximately 8 meters and reaches up to 13 meters in the Normand-Breton Gulf area (Mont Saint Michel Bay, northwest of France). This region is well known to be subject to strong wetting and drying (Service Hydrographique et Océanographique de

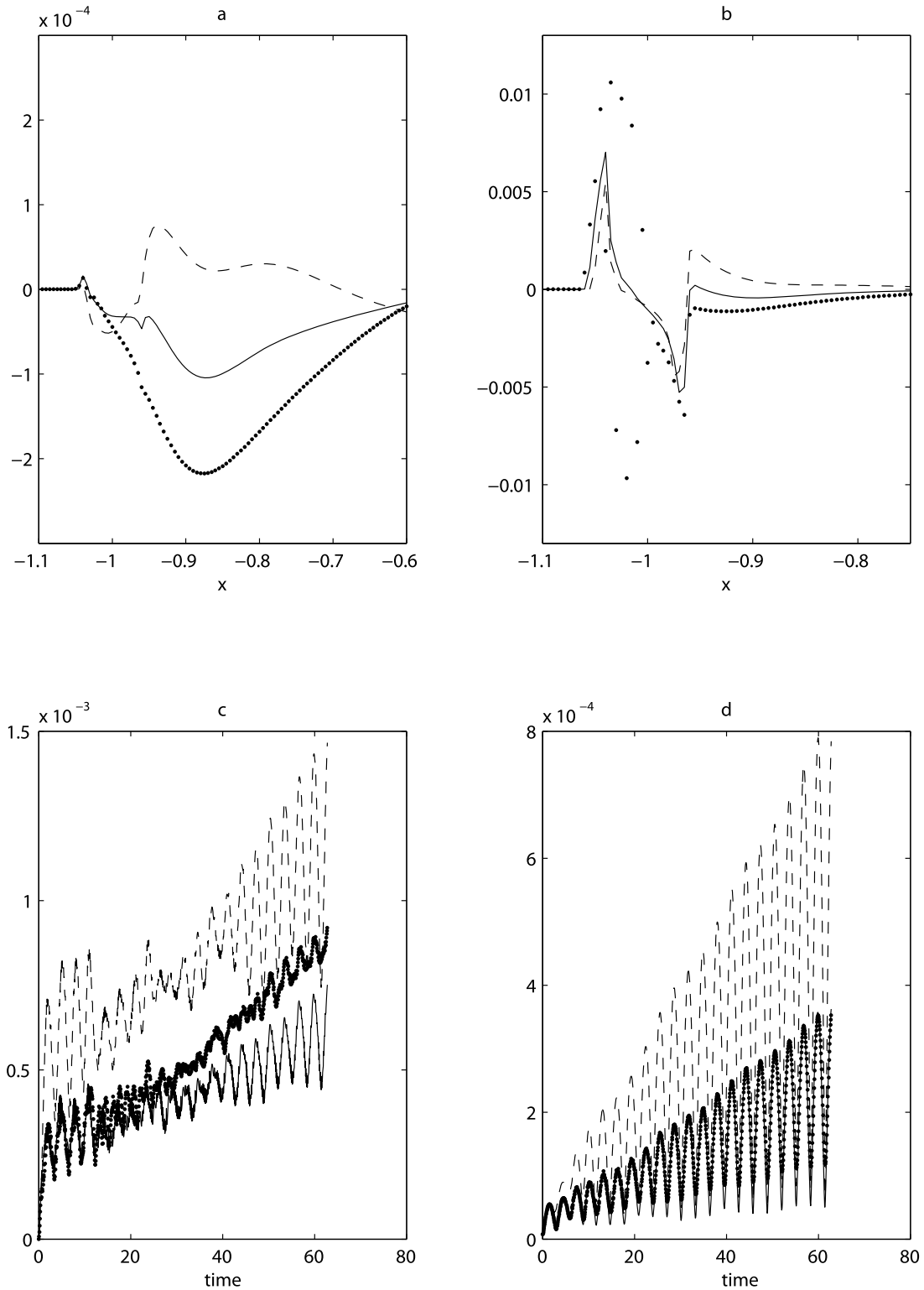


Figure 9. Sensitivity of the error with respect to the analytical solution for different choices. The solid line is $\alpha = 2$ (reference experiment), the dashed line is $\alpha = 4$, and the dotted line is $\alpha = 1$. The considered fields are (a) the mean alongshore velocity, (b) the mean alongshore transport, (c) the time evolution of the root mean square of the thickness, and (d) the time evolution of the root mean square of the alongshore transport.

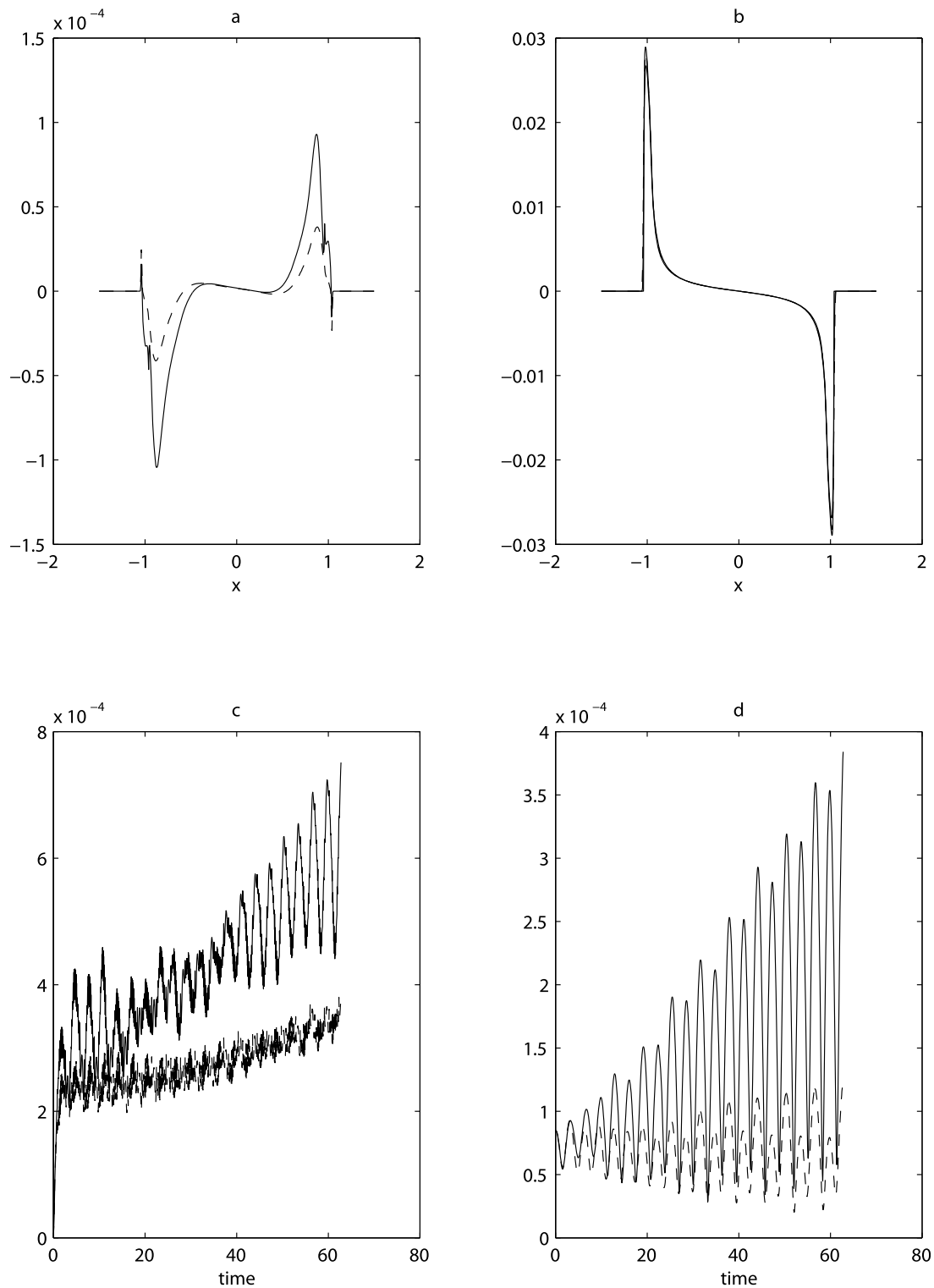


Figure 10. Same as Figure 9 but for α^U .

la Marine (SHOM), <http://www.shom.fr/>). In this area, for high tide coefficients, the sea can uncover more than 10 km, and some of the strongest tidal currents are found: up to 5 m/s in the Raz Blanchard region at the northwestern tip of the Cotentin peninsula.

[45] The HYCOM model [Bleck, 2002] has been modified to include the previous aforementioned wetting and drying

schemes. This model is called HYCOM-WD. It has been used to simulate tidal dynamics in the Normand-Breton Gulf area, in particular the strong wetting and drying conditions at the Mont Saint Michel Bay. Only one homogeneous layer is used (i.e., barotropic ocean) with a realistic bottom topography described in Figure 11.

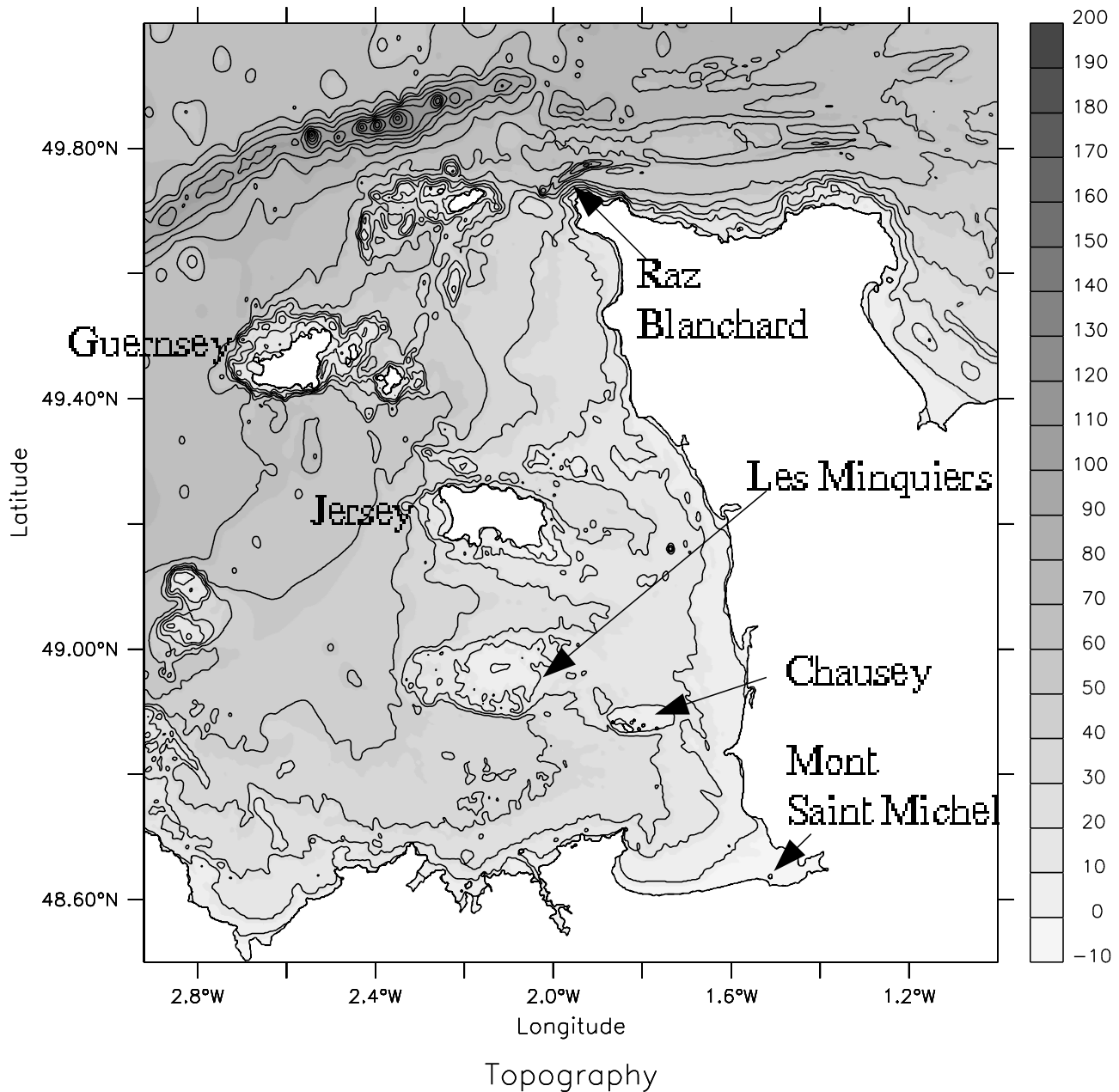


Figure 11. Topography of the Normand-Breton Gulf area, referenced to the mean level depth and built with the SHOM bathymetry and tide database. The land mask is in white.

[46] The model is projected on a Mercator grid with a model grid step varying from $\Delta X = 140$ m to $\Delta X = 150$ m. The ocean dynamic only takes into account the tidal forcing which is prescribed at the open boundaries using harmonic modes from the MOG2D tide model [Carrère and Lyard, 2003]. Special boundary conditions have been implemented in the HYCOM-WD based on Lax [1972] and Roe [1981]. They show that, if we suppose that the gravity waves at the boundary are faster than the advection, the boundary problem is well posed only if we impose one variable at the boundary (e.g., SSH, normal velocity or mass flow). The other variable is then deduced by the resolution of a Riemann problem at the boundary [Lax, 1972]. The realistic configuration described in this study uses a relation of flow conservation as well as a

relation coming from the shock/rarefaction curves of the homogeneous shallow water system, written with respect to the normal velocities and height [Roe, 1981].

[47] The starting time of the model simulation is 10 September 1997 and has the corresponding sea elevation and velocity field to have the correct mass. The model is run for 15 days. We choose this specific time to simulate the tides on 19 September 1997 which corresponds to a large tide coefficient as it reached 116, for a maximum theoretical coefficient of 120. The model is run with baroclinic and barotropic time steps of 12 and 1.5 s, respectively, and also uses a new time stepping scheme for the slow part of the barotropic mode described by Morel *et al.* [2008]. The baroclinic time step is needed despite the barotropic ocean

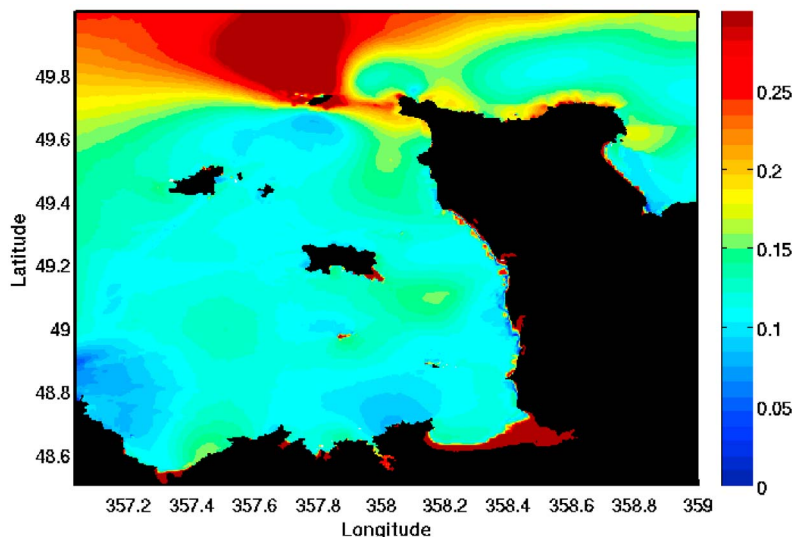


Figure 12. Relative error (equation (22)) in the Normand-Breton Gulf for the M_2 tide.

because in HYCOM the barotropic contribution of the advection and the diffusion is added in the baroclinic momentum equations. The harmonic analysis is carried out over 30 tidal periods. The bottom friction is formulated using a quadratic law given by equation (6) with $C_d = 3 \times 10^{-3}$.

4.2. Tidal Dynamics in the Normand-Breton Gulf

[48] MARMONDE is a system (developed at the SHOM) yielding estimates of SSH from combinations of tidal gauge measurements and output of a model calibrated on the English Channel [Simon, 2007]. MARMONDE has a resolution of one minute at the coast and approximately five minutes elsewhere. The high density of observations at the coast improves greatly its resolution but MARMONDE cannot be considered as perfect and its uncertainties are difficult to evaluate (no data apart from the tide gauges that are already integrated in MARMONDE). MARMONDE does not conserve mass or momentum due to the nudging and optimal interpolation of tidal amplitudes and phases to fit the available data. However, it is our best estimate in the area as it is the reference taken for hydrographic measurements in the Normand-Breton Gulf region. It is worthwhile to mention that MARMONDE has not been used to force the model at the open boundaries because it does not provide the velocity field which is necessary to ensure model mass conservation. The accuracy of the MARMONDE tidal data in the open ocean (i.e., our model open boundaries) is also not as accurate as in the coastal areas due to the sparse data. This is well shown in Figure 12 which is a spatial map of the relative error computed as follows:

$$\begin{aligned}
 R_x &= \eta_H^* \cos(\phi_H) - \eta_M^* \cos(\phi_M), \\
 R_y &= \eta_H^* \sin(\phi_H) - \eta_M^* \sin(\phi_M), \\
 R_{err} &= \frac{\sqrt{R_x^2 + R_y^2}}{\eta_M},
 \end{aligned} \tag{22}$$

with η_H and η_M as the M_2 tidal amplitudes for HYCOM-WD and MARMONDE, respectively, and ϕ_H and ϕ_M as

the M_2 tidal phases for HYCOM-WD and MARMONDE, respectively.

[49] Most of the error can be seen at the northern boundary, inside the domain and in our area of focus, the error represent about 10% of the total signal. The relative error (R_{err}) integration over the domain gives approximately a 10.6% error in the Normand-Breton Gulf.

[50] In this region, the most important tidal harmonics are M_2 and S_2 . Figure 13 shows the M_2 tidal amplitudes (Figure 13a), the M_2 tidal phases (Figure 13b), and the differences between those (Figure 13c) and the MARMONDE model (Figure 13d). As Figure 12 shows, most of the error can be attributed to the model open boundaries. At the coast, the model has about 0.2 m error (compare to a 4 m total tidal amplitude) and about a 5 degrees difference which represent an error of about ten minutes for the M_2 tidal constituent. The HYCOM-WD simulations results are in a very good agreement with the MARMONDE results as these errors are quite small. The main differences, seen at the boundaries, comes from the mass fluxes provided by the MOG2D model [Carrère and Lyard, 2003], which also has its own uncertainties.

[51] An harmonic analysis for the tidal wave MS_4 (resulting from the nonlinear interaction between M_2 and S_2) shows that its amphidromic point, located near the Guernsey island, is mislocated and shifted compare to the MARMONDE solution (not shown here). This is due to the forcing at the boundary which is located very close to this amphidromic point and also because a fine tuning of the intensity of the bottom friction is necessary to get accurate solutions for the MS_4 tidal wave.

[52] As the goal of this paper is not to do an exhaustive and extensive validation of the tide, we have, through the results presented above, confidence to pursue the tests of the wetting and drying scheme.

4.3. Wetting and Drying Areas

[53] Figure 14 shows a comparison between the SSH simulated with the HYCOM-WD model forced at the

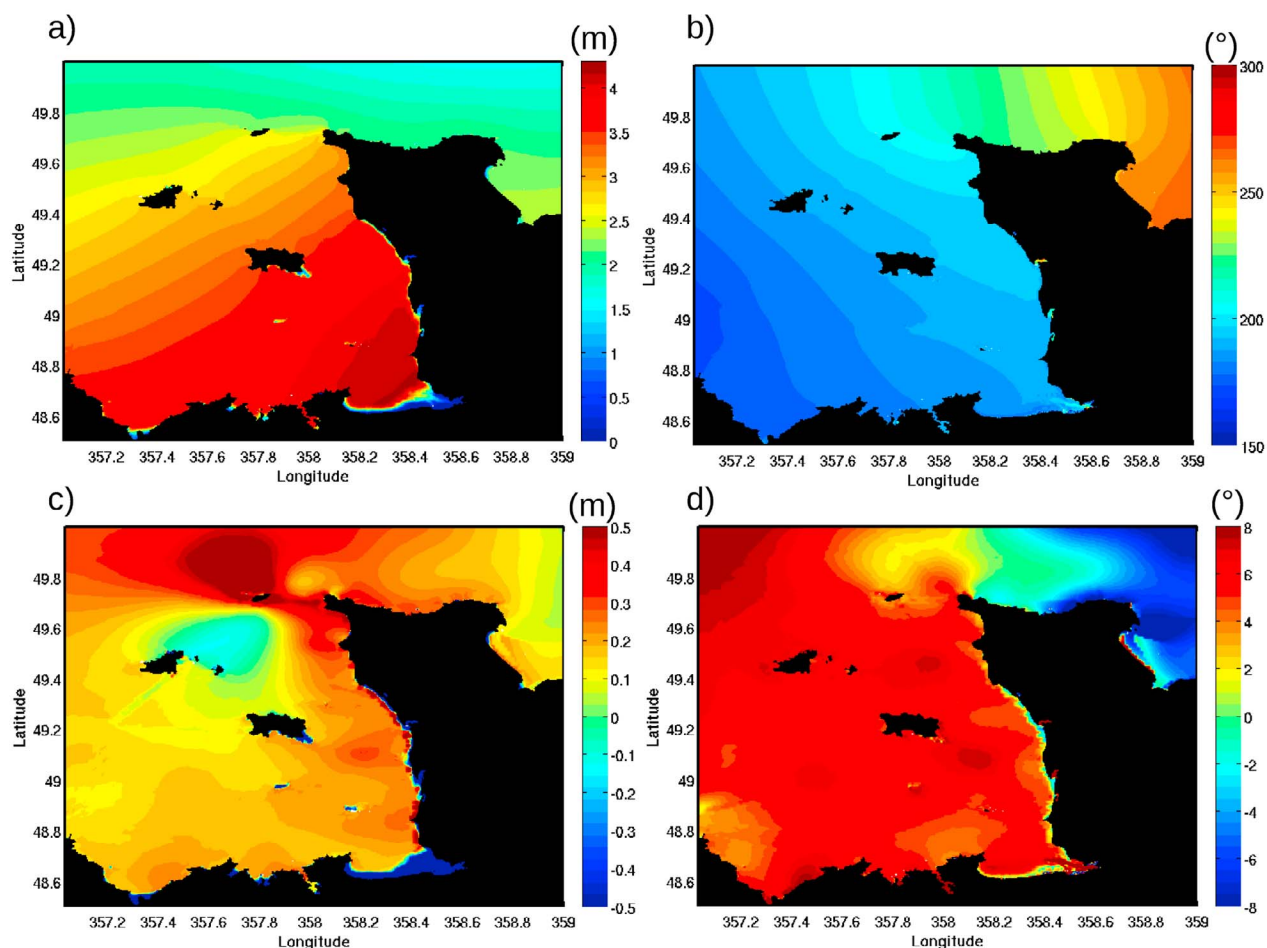


Figure 13. Numerical solutions of HYCOM-WD for M_2 tidal (a) amplitudes and (b) tidal phases in the Normand-Breton Gulf area. The M_2 differences between HYCOM-WD and MARMONDE for (c) tidal amplitudes and (d) tidal phases are also shown.

boundaries with 14 tidal wave (M_2 , S_2 , N_2 , K_2 , K_1 , O_1 , P_1 , Q_1 , M_4 , MS_4 , MN_4 , $2N_2$, M_3 , M_6) and the SSH retrieved from La Chapelle Saint Aubert tide gauge, located close to the Mont Saint Michel ($1^\circ52' W$, $48^\circ63' N$). The water is only present at this location when there is large tidal coefficient (e.g., the extreme event on 19 September 1997). The SSH is mainly influenced by the tidal signal in this area, although other processes such as atmospheric pressure, can also have a significant impact and are not taken into account in our simulations. Figure 14 shows that this area is generally dry (0 m line) except for a few hours between 15 and 22 September 1997. The amplitude errors can be significant, especially on 15 September. These differences can be explained by peculiar weather (e.g., strong winds) but not only: the inverse barometer effect, the model resolution and thus the local topography could also be responsible for those discrepancies between numerical solutions and observations. However, there is generally a good agreement between the simulated amplitudes of the model and those predicted by the tide gauge. Notice that there is no phase error, and that the duration for which the tide gauge records the presence of water is also well reproduced by the model. The evolution

and weakening of this extreme event is also quite well represented in the model.

[54] Figure 15 presents the whole domain with the permanently immersed zones (the height of water is always higher or equal to 10 cm, white) and areas periodically dried (gray) for the MARMONDE system and for the HYCOM-WD model, respectively. We observe a very good agreement between the two models. In particular, the drying zones of the islands of Guernsey, Jersey and Chausey ($1^\circ83' W$, $48^\circ88' N$) are similarly reproduced in the two models. The drying zone of the Minquiers plateau ($2^\circ13' W$, $48^\circ97' N$) is however too large in the HYCOM-WD, as is the western extension of the Seine bay. Figure 16 is the same as Figure 15 but zoomed on the bay of the Mont Saint Michel. It allows for a better comparison between the two models results. The black solid curve delimits a zone for which the height of water remains always strictly positive and delimits thus the minimal extension of the drying zone. The drying zone simulated by MARMONDE is within the two zones delimited by $0 < h < 10$ cm in HYCOM-WD, except for the channel of the See and Selune rivers ($1^\circ59' W$, $48^\circ69' N$), which are not represented in MARMONDE due to its lack

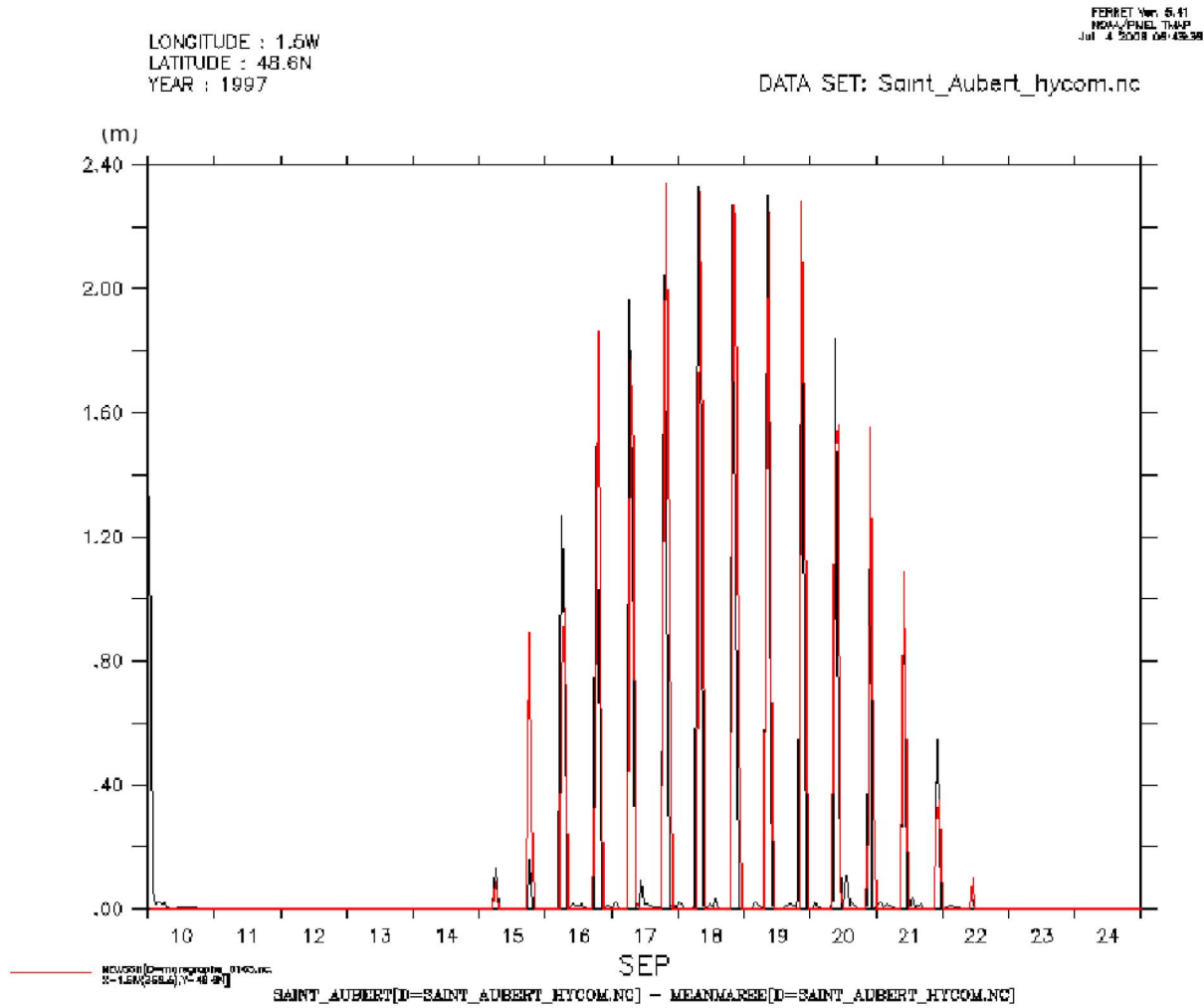


Figure 14. Comparison between the HYCOM-WD simulated SSH (*m*) (black line) and the SSH (*m*) retrieved by tidal gauge observations (red line) at La Chapelle Saint Aubert, near Mont Saint Michel.

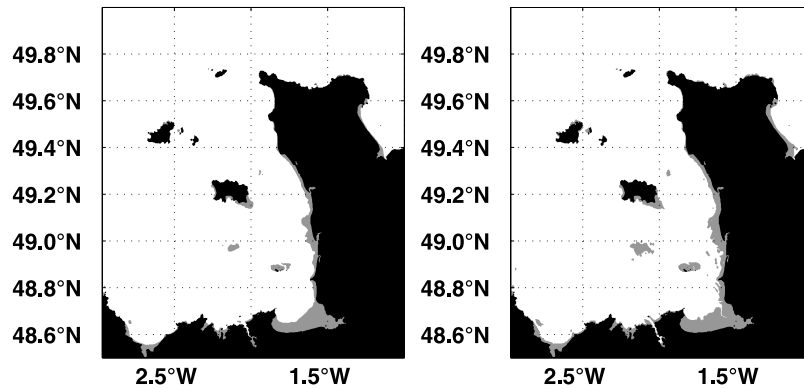


Figure 15. Wet area (white) and periodically dry area (gray) simulated by the (left) MARMONDE model and (right) HYCOM-WD model. A point is considered periodically dry when its water depth reaches less than 10 cm during the 15 day simulation between 10 and 25 September 1997.

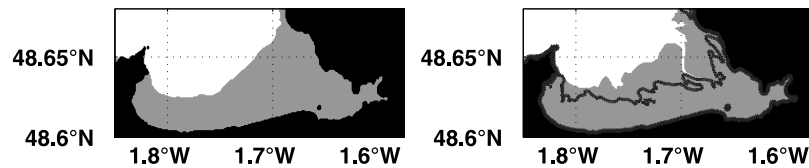


Figure 16. Same as Figure 15 but zoomed in on the Mont Saint Michel area. The black curve delimits the area where the water depth reaches 0 during the 15th simulation day.

of resolution. These results validate the wetting and drying schemes developed and implemented in HYCOM.

5. Discussion

[55] In this paper, we have proposed numerical schemes to take into account the wetting and drying processes suitable for oceanic circulation models that use finite difference methods. The numerical schemes are based on existing schemes, developed to deal with vanishing layers in isopycnic models, with some improvements. Different parameters have been defined, associated with critical depths, and has been optimized using Thacker's exact solutions for parabolic basins. Other shapes could yield different parameters, but we expect weak differences as long as the topography of the considered region is smooth enough. The critical depths are based mainly on two crucial parameters: the grid step and the local slope and is defined as: $h_c = 2s\Delta x$. Since, in the general case for realistic bottom topographies, our criterion for stability is based on the steepest local slope, an unsmooth topography will add more constraint to obtain stability and thus results could be less accurate.

[56] A realistic simulation have been performed in the Normand-Breton Gulf area and shows that the wet and dry areas are very well represented for the case of a strong tide.

[57] This study is also original as it concentrates on the simulated velocity fields. Those are challenging to get accurately as their evolution is associated with shocks. Our study shows that the numerical scheme captures very well the magnitude of the velocities. The algorithms we have used have been intensively studied and validated in the baroclinic case and they are very well known for their robustness and excellent ratio accuracy/computational efficiency (compare to Godunov methods for example). In this paper, it has been demonstrated that the proposed numerical scheme to represent the wetting and drying process conserves all those properties.

[58] The wetting and drying scheme mainly acts on the velocity field by doing some relaxation to it but conserves mass (and volume). It can thus be coupled with tracer evolution equations and, provided they are written in flux form, maintain their conservation properties, which is crucial for long-term simulations. For the baroclinic case, the conservation of tracers can be affected by the splitting of the external and internal mode (this is the case in HYCOM for instance), but including the present wetting and drying scheme in a code that conserves tracers can be done while preserving conservation. This property gives a strong consistency and portability between the algorithm and the model from a numerical and computational point of view.

[59] Although this work shows some original approach that could lead to considerable improvements for the finite

difference oceanic general circulation models, the results can be undoubtedly improved and several factor have to be considered to achieve more accurate solutions.

[60] 1. As discussed in the paper, for tidal simulations, the solution chosen at the boundary have a strong impact on the accuracy of the solution over the whole domain. For non-linear harmonics, this is also true for small regions, but some other parameters, in particular the bottom friction, have to be carefully tuned. In this respect, the barotropic (i.e., one layer) results we described would probably be improved using many layers and a more adequate parameterization for bottom boundary layers.

[61] 2. The precision of the bottom topography is also a key factor. The bathymetry not only acts on the precision of the propagation of tidal waves, but also on the bottom slope which is an essential factor to simulate accurately the local currents, which eventually act on the wetting and drying process.

[62] 3. Atmospheric forcing can also play a role in the surface height evolution, both through direct pressure effects or the influence of the wind.

[63] 4. The initial condition, and in particular the position of the sea surface (or a precise knowledge of the mean surface elevation), is of importance to achieve a good matching between numerical results and observations.

[64] 5. An increased resolution should also improve the numerical solutions. In the realistic study, there are only five grid points between the Mont Saint Michel and the coast, where the comparison with the tide gauge have been performed. In this case the results are also sensitive to the solid wall boundary conditions.

[65] The results (i.e., robustness, stability, and accuracy) we have obtained are encouraging and we believe that the numerical schemes presented here can be used for realistic and operational modeling.

[66] Finally, the choice and optimization of the parameters hc and ϵ could be extended to isopycnic layers when they encounter bottom topography. Using a baroclinic ocean would be an interesting experiment to perform since the time-splitting mode would affect the conservation of mass and tracers. This could be compared to Thacker's solutions that can easily be extended to stratified cases (the solution have the same shapes with identical barotropic velocity fields and isopycnals remaining parallel to the sea surface). The critical depths in MICOM and HYCOM have been fixed to 10 m whereas results from the present study show that there should be a strong dependence on the local bottom gradient and grid step.

[67] **Acknowledgments.** Sebastien Lahaye is supported by the CEA (Commissariat à l'Énergie Atomique). Flavien Gouillon is supported by

the ANR grant ANR-08-BLAN-0330-01. Annick Pichon, Lucia Pineau-Guillou, Remy Baraille, and Yves Morel are supported by the French Ministry of Defense and this work is part of the research program MOUTON (PEA 012401), funded by DGA, the French Navy, EPIGRAM funded by CNRS/LEFE/IDAO, and ANR (ANR-08-BLAN-0330-01). The project is conducted by SHOM, the French Navy Hydrographic and Oceanographic Service.

References

- Arakawa, A., and V. Lamb (1977), Computational design of the basic dynamical processes of the UCLA general circulation model, *Methods Comput. Phys.*, *17*, 174–267.
- Aureli, F., A. Maranzoni, P. Mignosa, and C. Ziveri (2008), A weighted surface-depth gradient method for the numerical integration of the 2D shallow water equations with topography, *Adv. Water Resour.*, *31*, 962–974.
- Balzano, A. (1998), Evaluation of methods for numerical simulations of wetting and drying in shallow water flow models, *Coastal Eng.*, *34*, 83–107.
- Bates, P. D., and M. S. Horritt (2005), Modelling wetting and drying processes in hydraulic models, in *Computational Fluid Dynamics: Applications in Environmental Hydraulics*, edited by P. D. Bates, S. N. Lane, and R. I. Ferguson, chapt. 6, pp. 121–146, John Wiley, Chichester, U. K.
- Begnudelli, L., and B. F. Sanders (2006), Unstructured grid finite-volume algorithm for shallow-water flow and scalar transport with wetting and drying, *Am. Soc. Civ. Eng. J. Hydraul. Eng.*, *132*, 371–384.
- Benkhaldoun, F., and L. Monthe (1994), An adaptive nine-point finite volume Roe scheme for two dimensional Saint-Venant equations, in *Modelling of Flood Propagation Over Initially Dry Areas*, edited by P. Molinaro, pp. 30–44, Am. Soc. of Civ. Eng., New York.
- Bleck, R. (2002), An oceanic general circulation model framed in hybrid isopycnic-Cartesian coordinates, *Ocean Modell.*, *4*, 55–88.
- Bleck, R., and B. Boudra (1986), Wind-driven spin-up eddy-resolving ocean models formulated in isopycnic and isobaric coordinates, *J. Geophys. Res.*, *91*, 7611–7621.
- Bleck, R., and L. Smith (1990), A wind-driven isopycnic coordinate model of the north and equatorial Atlantic Ocean: 1. Model development and supporting experiments, *J. Geophys. Res.*, *95*, 3273–3285.
- Bleck, R., C. Rooth, D. Hu, and L. Smith (1992), Salinity driven thermocline transients in a wind and thermohaline forced isopycnic coordinate model of the North Atlantic, *J. Phys. Oceanogr.*, *22*, 1486–1505.
- Bradford, S. F., and B. F. Sanders (2002), Finite-volume model for shallow water flooding of arbitrary topography, *Am. Soc. Civ. Eng. J. Hydraul. Eng.*, *128*, 289–298.
- Carrère, L., and F. Lyard (2003), Modeling the barotropic response of the global ocean to atmospheric wind and pressure forcing: Comparisons with observations, *Geophys. Res. Lett.*, *30*(6), 1275, doi:10.1029/2002GL016473.
- Cushman-Roisin, B. (1994), *Introduction to Geophysical Fluid Dynamics*, 320 pp., Prentice-Hall, Englewood Cliffs, N. J.
- Hervouet, J., and J. Janin (1994), Finite element algorithms for modelling flood propagation, in *Modelling of Flood Propagation Over Initially Dry Areas*, edited by P. Molinaro, pp. 101–113, Am. Soc. of Civ. Eng., New York.
- Lax, P. D. (1972), *Hyperbolic Systems of Conservation Laws and the Mathematical Theory of Shock Waves*, CBMS-NSF Reg. Conf. Ser. Appl. Math., vol. 11, Soc. for Ind. and Appl. Math., Philadelphia, Pa.
- Lazure, P., and A. M. Jegou (1998), 3D modelling of seasonal evolution of Loire and Gironde plumes in the Bay of Biscay continental shelf, *Oceanol. Acta*, *21*, 165–182.
- Lazure, P., and J.-P. Salomon (1991), Coupled 2D and 3D modelling of coastal hydrodynamics, *Oceanol. Acta*, *14*, 173–180.
- Leclerc, M. L., J. Bellemare, G. Dumas, and G. Dhatt (1990), A finite element model of estuarine and river flows with moving boundaries, *Adv. Water Resour.*, *13*, 158–168.
- Lynch, D. R., and W. G. Gray (1980), Finite element simulation of flow in deforming regions, *J. Comput. Phys.*, *36*, 135–153.
- Lynett, P., T. S. Wu, and P. Liu (2002), Modeling wave runup with depth-integrated equations, *Coastal Eng.*, *46*, 89–107.
- Morel, Y., R. Baraille, and A. Pichon (2008), Time splitting and linear stability of the slow part of the barotropic component, *Ocean Modell.*, *23*, 73–81.
- Oey, L. Y. (2005), A wetting and drying scheme for POM, *Ocean Modell.*, *9*, 133–150.
- Oey, L. Y. (2006), An OGCM with movable land-sea boundaries, *Ocean Modell.*, *13*, 176–195.
- Roe, P. L. (1981), Approximate Riemann solvers, parameter vectors and difference schemes, *J. Comput. Phys.*, *43*, 357–372.
- Simon, B. (2007), *La Marée Océanique Côtière*, 443 pp., Inst. Oceanogr., Paris.
- Smagorinsky, J. S. (1963), General circulation experiments with primitive equations. Part I: The basic experiment, *Mon. Weather Rev.*, *91*, 99–164.
- Smolarkiewicz, P. (1983), A simple positive definite advection scheme with small implicit diffusion, *Mon. Weather Rev.*, *111*, 479–486.
- Thacker, W. (1981), Some exact solutions to the nonlinear shallow-water wave equations, *J. Fluid Mech.*, *107*, 499–508.
- van't Hof, B., and E. Vollebregt (2005), Modelling of wetting and drying of shallow water using artificial porosity, *Int. J. Numer. Methods Fluids*, *48*, 1199–1217.
- Winther, N., Y. Morel, and G. Evensen (2007), Efficiency of high order numerical schemes for momentum advection, *J. Mar. Syst.*, *67*, 31–46.
- Zalesak, S. (1979), Fully multidimensional flux-corrected transport algorithms for fluids, *J. Comput. Phys.*, *3*, 335–362.

R. Baraille, F. Gouillon, and Y. Morel, SHOM, HOM, 42 Ave. Gaspard Coriolis, Site de Météo-France, F-31057 Toulouse, France. (flavien.gouillon@shom.fr)

S. Lahaye, CEA/DEN, Centre de Saclay, PC 57, F-91191 Gif-sur-Yvette CEDEX, France.

A. Pichon and L. Pineau-Guillou, SHOM, HOM, 13 Rue du Chatellier, CS 92803, F-29228 Brest CEDEX 2, France.